Simulation study of helium bubble coalescence in tungsten at various temperatures relevant to fusion conditions

Simulation study of helium-bubble coalescence in tungsten at various temperatures relevant to fusion conditions

*Jie Zhan [a, b] *, Taira Okita[b], Minyou Ye[a], Daiji Kato[c], and Katsuyuki Suzuki[b]*

[a]Department of Engineering and Applied Physics, School of Physical Sciences, University of Science and Technology of China, Hefei 230026, China

[b] School of Engineering, University of Tokyo, 7-3-1 Hongo, Bunkyo, Tokyo 1138656, Japan

[c]National Institute for Fusion Science, 322-6 Oroshi, Toki, Gifu 5095292, Japan

Abstract

Molecular dynamics (MD) methods are used to study nanosized helium (He) bubble coalescence process in tungsten (W) at various temperatures relevant to fusion conditions, on an atomistic scale. Bubble coalescence in W is observed at a higher temperature and He/V ratio, while the calculated internal bubble pressure due to virial stress increases with the increase in the He/V ratio; bubble coalescence is significantly dependent on the bubble distance. In these MD simulations, coalescence occurs, only when the surface distance between the two bubbles is equal to $1a_0$, where a_0 denotes the lattice constant and is approximately 0.317 nm at 2100 K. On the other hand, a bubble diameter between $1a_0$ and $3a_0$ may have relatively limited effect on the coalescence, although larger-sized bubbles may have higher migration energy. Physical contact may occur between two nearby bubbles at the initial stage of coalescence accompanied by W lattice distortion because of the limited displacement of W atoms near the bubbles and rapid migration of He atoms within the two bubbles. These results are beneficial for understanding the evolution of He bubbles in bulk W.

Keywords: Molecular dynamics, Plasma facing materials, Helium implantation, Bubble interaction

1. Introduction

In nuclear fusion devices, tungsten (W) with its excellent thermophysical and mechanical properties has been used as the PFM for plasma facing components such as the first wall and divertor plate [1-3], which are subjected to high temperature, and high flux plasma (10^{21}－10^{24} $m^{-2}s^{-1}$) and high energy neutron exposure (approximately 14 MeV) [4,5]. It is well known that insoluble-gas helium (He) atoms produced as a result of He plasma irradiation and (n, α) nuclear transmutation reactions lead to the formation of nanosized bubbles [6,7]; this has been experimentally observed in various metals [8-11]. The bubbles and their evolution play an important role in the performance of W as the PFM in fusion devices because they can cause drastic degradation of W properties such as the ductility and thermal conductivity [12-14]. Therefore, understanding the behavior of He bubbles in W is fundamental for the design of W materials in fusion devices. Two distinct mechanisms have been proposed for the growth of small He bubbles

---

Plasma Facing Material (PFM)
Molecular Dynamics (MD)
Density Functional Theory (DFT)
Wigner Seitz (WS)
EMBEDDED ATOM METHOD (EAM)
Common Neighbor Analysis (CNA)

[10]: one is migration and coalescence, which indicates that entire bubbles can move randomly through the stochastic formation of Frenkel pairs and helium fluxes, coalescing and growing into larger-sized bubbles when the bubbles meet. The other mechanism is the Ostwald ripening mechanism, where He atoms and vacancies can dissociate from smaller-sized bubbles, in particular, and diffuse into the other existing bubbles. Although several studies have investigated these mechanisms [15,16], on an atomistic scale, they are required to be further understood.

Atomistic simulation techniques such as MD and DFT are important complementary tools [17-19] extensively applied to study He defect energetics, interactions between He and the defects, He effect on the lattice thermal conductivities, and He bubble evolution near the surface or in a matrix [20-22]. B.D. Wirth et al. investigated the evolution and distribution of He clusters or small He bubbles with He atom numbers up to several tens near the W surface using MD simulations [23]. However, the coalescence of bubbles with diameters greater than 1 nm in the W matrix has not yet been well simulated.

In this study, we investigate the coalescence process of two nanosized bubbles at several bubble distances in the W matrix over a wide temperature range relevant to fusion conditions through MD simulations. The effect of bubble pressure corresponding to the He/V ratio is studied, along with the analysis of the distorted W surrounding high-pressure bubbles. In order to understand the bubble coalescence mechanism, we observe the trajectories of typical He and W atoms, and calculate the local pressure profile near the He bubbles.

2. Simulation Methods

MD simulations were employed for studying the coalescence process of two nanosized bubbles in the W matrix, using the open-source program LAMMPS [24]. In these computations, the W-W interactions were described using the EAM potential of Ackland and Thetford [25]. The pair-wise interactions of W-He and He-He were described according to the pair potential of Juslin and Wirth [26], and Beck [27], respectively.

In all the simulations, the simulation cell was a $20a_0 \times 20a_0 \times 20a_0$ block of perfect bcc-W with the x, y, and z axes of the simulated crystal oriented along the [10 0], [0 1 0], and [0 0 1] directions, respectively. Periodic boundary conditions in all the three axial directions were used throughout the simulations and a time step of 1 fs was applied. In order to determine the lattice constant a_0 at several temperatures, NPT ensemble simulations were performed at certain temperatures ranging from 300–2100 K. Thus, in all the simulations in this study, the lattice constant change due to the thermal expansion effect has been considered. All the simulation cell lengths remained constant when the NVT ensemble was used for 1.5 ns to evolve the W matrix containing two nanosized bubbles constructed with identical size. The Nosé-Hoover thermostat method was used to control the temperature [28]. Because of the higher migration energy and the resultant lower diffusion coefficient of the nanosized He bubble, the bubble distance, defined hereafter as the closest surface distance between two bubbles, was set to range from $1a_0$–$3a_0$ to facilitate their physical touch within the MD simulation time. In order to study the effect of over-pressurized as well as under-pressurized bubbles, the He/V ratio was varied from 1–3 because the equilibrium He/V ratio was calculated to be approximately two for a nanosized bubble in the W bulk [29]. To obtain good statistical bubble coalescence results, simulations were conducted at least six times for each condition. The occurrence possibility of bubble coalescence was then calculated in each case.

The WS cell method was applied to analyze defect cluster behavior, such as vacancies and W interstitial atoms [30]. In addition, W lattice distortion caused by the bubbles was analyzed applying the statistics of CNA [31] to obtain insight into the microscopic mechanism of the coalescence of two bubbles on an atomistic scale. In order to evaluate the effect of bubble pressure, the internal bubble pressure at different He/V ratios was calculated using the Virial stress [32], and the trajectories of the displaced atoms and local profile of the atomistic stress were observed.

3. Results and discussion

3.1. Condition for bubble coalescence

We first studied the occurrence of bubble coalescence under several conditions, such as various bubble sizes, bubble distances, He/V ratios, and temperatures. The initial bubbles were set as spherical with radii ranging from $1a_0$–$3a_0$, corresponding to a maximum diameter of approximately 2 nm. For investigating the effect of bubble pressure, the virial stress in the bubble region, with various He/V ratios and bubble sizes, was calculated. Fig.1 depicts the calculated internal bubble pressure P_v as a function of the bubble size at 300 K. The equilibrium pressure of a spherical bubble P can be defined by the surface tension γ:
$P = 4\gamma/d$, where d is the bubble diameter. When the internal pressure exceeds the surface tension, the bubble has excess pressure $P_e = P_v - 4\gamma/d$, which may lead to loop punching or interbubble fracture [33]. As shown in Fig. 1, the calculated internal pressure ranges from 1.5–32.4 GPa for up to approximately 2-nm diameter bubbles with a He/V range of 1–3, and increases higher with the increase in the He/V ratio. However, in all the cases, the calculated pressure decreases with the increase in the bubble size at a fixed He/V ratio, which is in good agreement with the above-mentioned surface tension expression.

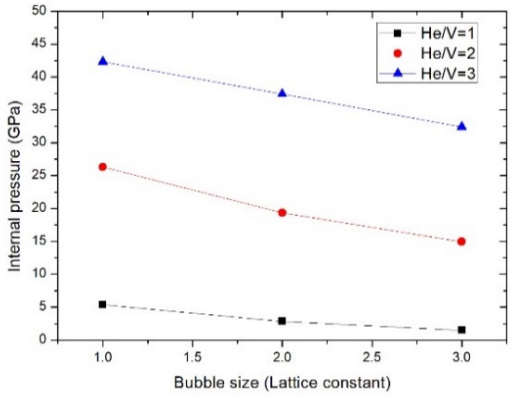

Fig. 1. Internal bubble pressure calculated at 300 K as a function of the bubble size (up to approximately 2-nm diameter) at various He/V ratios.

If the distance between the two He bubbles is less, coalescence may occur, which has been widely observed experimentally in metals [34,35]. In this study, we investigated nanosized He bubble coalescence in the W matrix for a wide temperature range relevant to fusion conditions. Bubble coalescence has significant impact on the spatial and size distribution of the bubbles in W, causing considerable changes in the W properties. Fig. 2 shows the coalescence process of two bubbles with diameters of 1.27 nm at 2100 K. The bubbles were constructed with a distance of approximately 0.317 nm between the nearest surface atoms and a He/V ratio of three. As shown in Fig. 2, at a high temperature of 2100 K, the bubbles start to touch each other rapidly within 0.3 ns. The large migration energy of the bubble in the W matrix results in considerably lower possibility for bubble diffusion within 0.3 ns; therefore, this may be caused by the interaction between the two bubbles. A the dumbbell-like structure comprising He atoms is formed after the two spherical bubbles contact, initially. However, within the remaining relatively longer 1.2 ns, the dumbbell-like bubble structure appears to remain steady. To understand the changes in the bubble structure during bubble coalescence, the number density of He atoms in the two bubbles was calculated, as depicted in Fig. 3. For the initial evolution time curve, the number density of He atoms in the area between the initial two bubbles is zero, indicating that there are no He

Initial 0.3 ns 0.6 ns

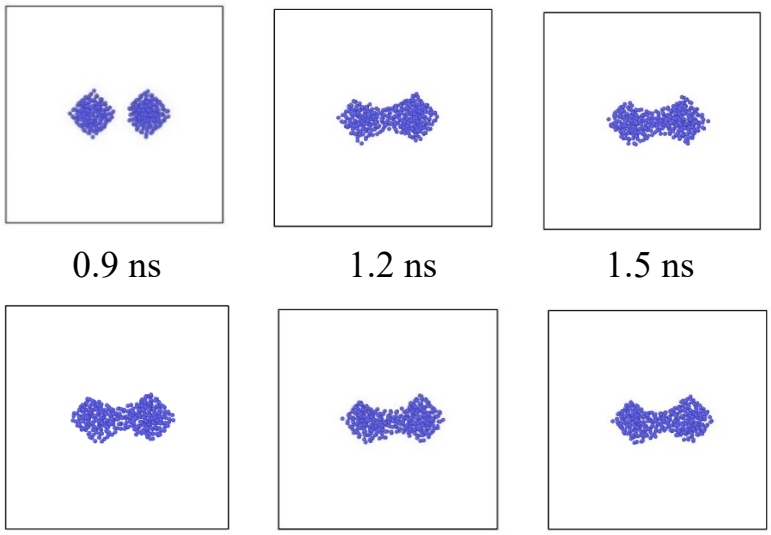

Fig. 2. Snapshots of bubble coalescence at a distance of approximately 0.317 nm at 2100 K.

atoms in the corresponding area. The number density curve becomes nonzero in the area between the initial two bubbles, when they are in physical contact and a dumbbell-like bubble structure is formed. Further, the changes in the curve are negligible in 1.2 ns, indicating that the bubble structure remains steady within the corresponding evolution time.

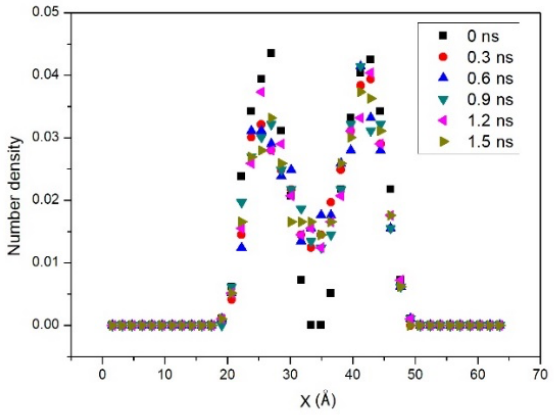

Fig. 3. Evolution of the number density of He atoms during the coalescence of two bubbles at a distance of approximately 0.63 nm at 2100 K.

The occurrence possibility of bubble coalescence during an evolution time of 1.5 ns at each condition are listed in Table 1 for different temperatures and He/V ratios. It can be observed that the probabilities increase with the increase in temperature and He/V ratio. Although a higher temperature increases the diffusion coefficient of He atoms and the possibility of coalescence, bubble coalescence was not observed, even at a high temperature 2100 K for He/V equal to or less than two. This may be because of the equilibrium He/V ratio of the bubbles (calculated to be approximately two), which necessitates a longer time than the evolution time of 1.5 ns for coalescence between the two bubbles. Table 2 shows the occurrence possibilities of coalescence between two bubbles with He/V=3 for different bubble sizes and distances at 2100 K. The results indicate that bubble coalescence occurs between the two bubbles, when the distance between them is as less as $1a_0$ (approximately 0.317 nm in all cases); however, bubble coalescence is difficult when the distance is equal to or more than $2a_0$ (approximately 0.63 nm), at least within the evolution time.

A smaller-sized bubble generally has lower migration energy and higher diffusion coefficient, but it is indicated that the effect of the bubble size may be relatively limited on bubble coalescence at least within R = 1a_0–3a_0 in the study.

Table 1 Occurrence possibility of bubble coalescence at different He/V ratios and temperatures ranging from 300–2100 K. The bubble distance and diameter are approximately 0.317 nm 1.26 nm, respectively.

Temperature (K)	He/V=1	He/V=2	He/V=3
300	0	0	0
900	0	0	0
1500	0	0	1/6
2100	0	0	6/6

Table 2 Occurrence possibility of bubble coalescence at different bubble distances and sizes. The temperature and He/V are approximately 2100 K and three, respectively. R is the bubble radius; D is the bubble distance.

R (a_0)	D=1a_0	D =2a_0	D =3a_0
1	6/6	0	0
2	6/6	0	0
3	6/6	0	0

3.2. Trajectory and W distortion

In order to understand the coalescence process of two He bubbles in W, the representative trajectories of the He atoms in the bubbles and the W atom displaced nearby are monitored for approximately 1.5 ns during bubble coalescence at 2100 K, as shown in Figs.4(a) and 4(b). For 1.26-nm diameter bubbles with He/V=3, it can be observed that only the W atoms between the two bubbles are displaced from their lattice sites, causing the He atoms in the bubbles to diffuse into the sites occupied by the W atoms. The W atoms between the two bubbles are rapidly displaced within the first 0.3 ns. However, the displaced W atoms generally remain steady further up to 1.2ns, which may be due to the steady structure of the bubbles after physical contact. Limited displacement of W atoms is observed within the evolution time of 1.5 ns only when bubble coalescence proceeds at a higher temperature of 2100 K, indicating that the displacement of W atoms around the bubble is significantly dependent on the nearby bubbles and temperature. The maximum displacement of He atoms around the bubbles was calculated to be approximately 2.305 nm on the (0 1 0) plane, which is considerably higher than that of W atoms at approximately 0.431 nm. Through the trajectories of the He atoms in the bubbles, it was determined that these atoms can migrate rapidly within the bubbles and across the middle of the two bubbles occasionally.

(a) (b)

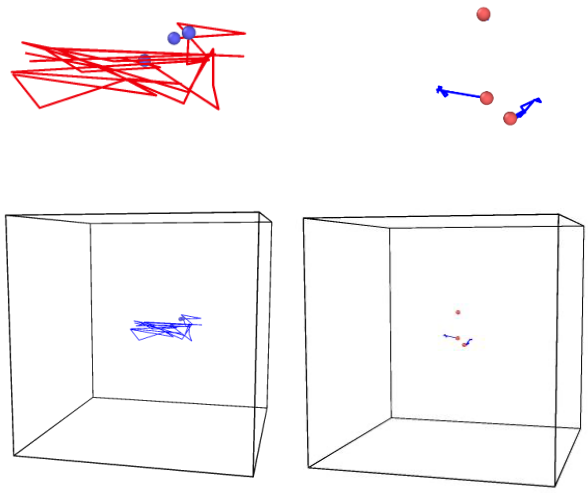

(c)

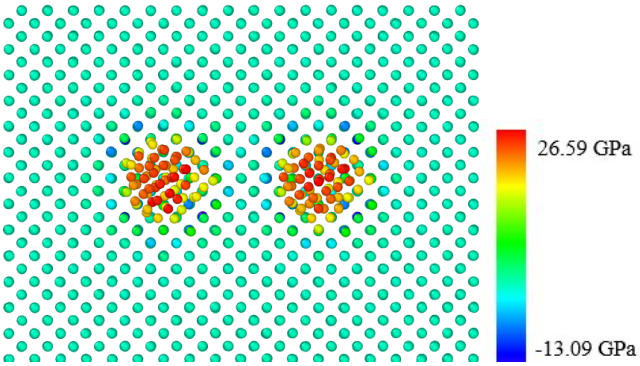

Fig. 4. (a) Representative trajectory of He atoms in the bubbles and (b) W atoms around the bubbles. The maximum displacements of the He and W atoms were calculated to be 2.305 nm and 0.431 nm on the (0 1 0) plane, respectively. (c) Atomistic pressure profile around the two 1.27-nm diameter bubbles.

The local atomic pressure profile around the 1.27-nm diameter He bubbles at a distance of 0.633 nm on the (0 1 0) plane is displayed in Fig. 4 (c). The pressure of W atoms around a bubble with He/V=2 is considerably higher than that located at a further distance due to the distortion caused by the bubbles; the pressure of all the W atoms were calculated to be in the -13.09–8.92 GPa range, in this case. It is indicated that two bubbles at a distance of 0.633 nm are likely to coalesce because there is a blue area between the bubbles. The pressure of the He atoms within the two bubbles were calculated to range from 12.83–26.59 GPa; the pressure of the He atoms near the bubble core were higher than those near the bubble surface. This may be due to the shell structure of the nanosized bubble in W, which is in good agreement with previous studies [29].

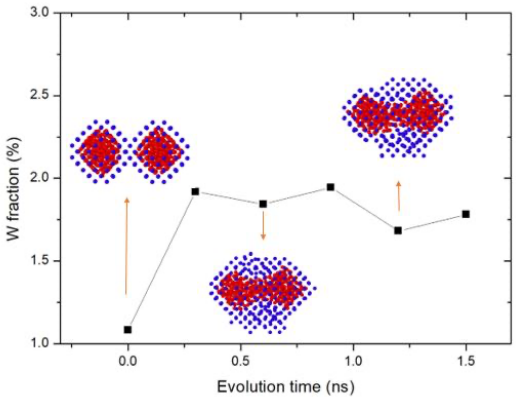

Fig. 5. Distorted W fraction, induced by the bubbles, with respect to the evolution time. Red denotes He atoms whereas blue denotes the distorted W atoms as per CNA analysis.

In Fig. 5, the fraction of distorted W atoms and snapshot of the matrix distortion induced by two He bubbles at 2100 K are depicted as a function of the evolution time. A significantly distorted matrix different from the bcc lattice structure is observed around high-pressure bubbles with He/V=3. The distorted W fraction is relatively lower when the bubbles are initially placed in the W matrix; after 0.3 ns, physical contact occurs between the bubbles and there is a sharp increase in the W fraction from 1.1% to 1.9%, which can be attributed to the distortion of the W lattice atoms between the two bubbles. However, within 1.2 ns, the W distortion generally remains unchanged, with a steady bubble structure. Compared to other metals such as iron, W has larger cohesive energy and equilibrium He/V ratio for the He bubbles, which may render bubble coalescence difficult.

4. Conclusions

The coalescence of two nanosized He bubbles in W was studied through MD simulations on an atomistic scale. In these simulations, bubble coalescence occurred even within the MD time scale of up to 1.5 ns, when the surface distance between two high-pressure bubbles was less than approximately 0.317 nm at 2100 K. However, it was observed that bubble diameters of up to approximately 2 nm had relatively limited effect on the coalescence. Analyses of the calculated pressure profile and W distortion around the bubbles indicated that bubble coalescence may be due to rapid He migration across the bubbles and the limited displacement of W atoms near the bubbles.

Acknowledgments

This work is supported by the National Key Research and Development Program of China (Grant No. 2017YFA0402500), Users with Excellence Project of Hefei Science Center CAS (2018HSC-UE010), Scholarship Fund of China Scholarship Council (201906340111), and by JSPS KAKENHI Grant Numbers JP17H03518, JP17KT0039 and JP20H02662. Numerical simulations were performed on the ITO supercomputer system of Kyushu university. The authors are grateful for the support.

References

[1] J.W. Davis, V.R. Barabash, A. Makhankov, L. Plochl, K.T. Slattery, J. Nucl. Mater. 308 (1998) 258–263
[2] G. Miloshevsky, A. Hassanein, Nucl. Fusion 54(4) (2014) 043016.
[3] R.E. Nygren, D.L. Youchison, R.D. Watson, S.O. Dell, Fus. Eng. Des. 49&50 (2000) 303.
[4] C.H. Wu, C. Alessandrini, J.P. Bonal, J.W. Davis, A.A. Haasz, W. Jacob, A. Kallenbach, J. Keinonen, P. Kornejew, R. Moormann, V. Philipps, J. Roth, F. Scaffidi-Argentina, H. Würz, Fus. Eng. Des. 56&57 (2001) 179.

[5] R. Behrisch, G. Federici, A. Kukushkin, D. Reiter, J. Nucl. Mater. 388 (2003) 313–316
[6] F.A. Garner, D.S. Gelles, L.R. Greenwood, T. Okita, N. Sekimura, W.G. Wolfer, J. Nucl. Mater. 329-333 (2004) 1008–1012
[7] T. Okita, W.G. Wolfer, F.A. Garner, N. Sekimura, J. Nucl. Mater. 329-333 (2004) 1013–1016
[8] M.Y. Ye, S. Takamura, N. Ohno, J. Nucl. Mater. 1243 (1997) 241–243
[9] D. Nishijima, M.Y. Ye, N. Ohno, S. Takamura, J. Nucl. Mater. 1029 (2004) 329–333
[10] P.J. Goodhew, Radiat. Eff. 78 (1983) 381–383.
[11] D. Aitken, P.J. Goodhew, M.B. Waldron, Nature 244 (1973) 15–16.
[12] D.E.J. Armstrong, P.D. Edmondson, S.G. Roberts, Appl. Phys. Lett. 102 (2013) 251901.
[13] S. Cui et al., J. Nucl. Mater. 486 (2017) 267–273.
[14] T. Miyazawa, T. Hwang, K. Tsuchida, T. Hattori, M. Fukuda, S. Nogami, A. Hasegawa, Nucl. Mater. Energ. 15 (2018) 154–157.
[15] C. González, R. Iglesias, J. Mater. Sci. 49 (2014) 8127.
[16] M. Callisti, M. Karlik, T. Polcar, J. Nucl. Mater. 473 (2016) 18–27.
[17] X.C. Li, Y.N. Liu, Y. Yu, G.N. Luo, X. Shu, G.H. Lu, J. Nucl. Mater. 451 (2014) 356–360.
[18] S. Miyashiro, S. Fujita, T. Okita, H. Okuda, Fusion Eng. Des. 87 (2012) 1352–1355
[19] K. Asari, O.S. Hetland, S. Fujita, M. Itakura, T. Okita, J. Nucl. Mater. 442 (2013) 360–364
[20] K. Doihara, T. Okita, M. Itakura, M. Aichi, K. Suzuki, Philo. Mag. 98 (2018) 2061–2076
[21] J. Zhan, M.Y. Ye, S.F. Mao, J.C. Ren, X.Y. Xu, Fusion Eng. Des. 146 (2019) 983–986.
[22] L. Hu, B.D. Wirth, D. Maroudas, Appl. Phys. Lett. 111 (8) (2017) 081902.
[23] F. Sefta, K.D. Hammond, N. Juslin, B.D. Wirth, Nucl. Fusion 53 (2013) 073015.
[24] S. Plimpton, J. Comput. Phys. 117 (1995) 1–19.
[25] G.J. Ackland, R. Thetford, Philos. Mag. A 56 (1987) 15.
[26] N. Juslin, B.D. Wirth, J. Nucl. Mater. 432 (2013) 61.
[27] D.E. Beck, Mol. Phys. 332 (1968) 15.
[28] G.J. Martyna, M.L. Klein, M. Tuckerman, J. Chem. Phys. 97 (1998) 2635.
[29] M. Y. Ye, J. Zhan, S. F. Mao, Z. Liu, Y. M. Ding, Fusion Eng. Des. submitted for publication.
[30] W. D. Wilson, C. L. Bisson, M. I. Baskes, Phys. Rev. B 24 (1981) 5616.
[31] D. Faken, H. Jonsson, Comput. Mater. Sci. 2 (1994) 2.
[32] M.P. Allen, D.J. Tildesley, Computer Simulation of Liquids, Oxford University Press, 1987.
[33] H. Evans, J. Nucl. Mater. 228 (1978) 76–77.
[34] K. Ono, K. Arakawa, K. Hojou, J. Nucl. Mater. 1507 (2002) 307–311
[35] K. Ono, S. Furuno, K. Hojou, T. Kino, K. Izui, O. Takaoka, N. Kubo, K. Mizuno, K. Ito, J. Nucl. Mater. 191 (1992) 1269–1273.